A data analysis procedure for phase identification in nanoindentation results of cementitious materials

F. Bernachy-Barbe

1 **Phase identification in high resolution nanoindentation results of cementitious materials**

2 *F. Bernachy-Barbe[1*]*

3 [1]Den-Service d'Etude du Comportement des Radionucléides (SECR), CEA, Université Paris-Saclay, F-

4 91191, Gif-sur-Yvette, France

5 *Corresponding author: fabien.bernachy-barbe@cea.fr

6 **Abstract**

7 Measuring accurately phase properties is essential for a realistic mesoscale modeling of materials, and

8 nanoindentation is a popular technique regarding mechanical properties. Given the statistical nature

9 of the grid indentation method, where large arrays of indents are performed blindly, the identification

10 of phases from the distributions of measured properties is an essential step. Many biases can be

11 introduced at that stage when the phases do not have very distinct properties as is often the case for

12 cementitious materials, since many indentation tests may also be in effectively heterogeneous areas.

13 It is proposed in the present work to analyze statistical indentation results on cementitious materials

14 with a hierarchical clustering algorithm making use of enriched information, including the spatial

15 coordinates of the indent. It is shown that it allows to reduce potential biases of the method by

16 eliminating tests in potentially heterogeneous areas and performing model independent identification

17 of the different phases.

18 Keywords

20 **1. Introduction**

21 Nanoindentation provides an efficient method to probe the mechanical properties of materials at

22 microscopic length scales. By applying force using an indenter of known geometry and properties onto

23 the surface of a sample, the obtained force-depth response is analyzed through contact mechanics in

order to commonly extract the local elastic modulus and hardness. In the context of cementitious materials, nanoindentation is being widely used, for example, to study Interfacial Transition Zones [1,2], chemical degradation [3] or carbonation [4], or time-dependant (creep) properties [5–8]. By directly measuring the elementary phases properties [9–13] nanoindentation allows for a direct experimental input to upscaling methods [14] that aim to increase their predictive capabilities in deriving effective mechanical properties.

The now standard phase identification procedure from nanoindentation data relies on the identification of a Gaussian Mixture Model (GMM) on the 2D distribution of indentation mechanical properties [15,16]. More descriptors such as chemical information can be added in these classification methods to identify phases more reliably coupling EDS and nanoindentation, where one can use in the procedure atomic ratios combined with indentation parameters [17–19]. For the standard approach making use only on micromechanical measurements, some controversy has arisen on the capabilities of the statistical indentation method to determine properties of single phases in cement paste [20,21], since the fitting of GMM presents many local minima [22]. More generally, it has been notably argued that in the nanoindentation testing of cementitious materials, probed volumes smaller than the heterogeneity length scale (possibly in pure phases) are too small relatively to the minimal obtainable roughness given by the porosity (where adequate contact conditions are fulfilled).

In view of these issues, it is proposed in the present work to take advantage of the spatialized nature of the data provided by nanoindentation maps in order to reduce these biases commonly introduced in the post-processing stage of statistical nanoindentation. It is first argued that the standard analysis of nanoindentation data based on Gaussian mixture models inevitably introduces biases when phases' mechanical properties do partially overlap. A post-processing method using more fully the obtained experimental data is proposed: after the removal of indentation tests where a local homogeneity criterion is violated, a hierarchical clustering algorithm making use of enriched and spatialized data is

2

1 used. An application to indentation results on a high water-to-cement ratio cement paste and hydrated

2 alite is presented.

2. Standard indentation methods

a. Analysis of load-displacement data

5 An instrumented indentation test consists in applying a force load path to the surface of a sample using

6 an indenter with precisely characterized properties, and recording the corresponding displacement

7 response of the indenter tip. This force-displacement data (assuming proper preliminary correction of

8 the indenter's compliance and detection of the contact point) is then subject to an inverse analysis

9 using contact mechanics, often with the Oliver and Pharr method [23]. The hardness H follows its usual

10 definition:

$$H = \frac{F_{max}}{A_c}$$

12 where F_{max} is the peak load and A_c the contact area under the indenter, obtained through f, the

13 indenter area function with $A_c = f(h_c)$. The contact depth h_c is obtained by correcting the measured

14 depth h for the displacement of the contact perimeter (sink-in), given by the solution of Sneddon for

15 the indenter elastic contact [24] :

$$h_c = h - \varepsilon \frac{F_{max}}{S}$$

17 where S is the elastic unloading stiffness. The ε coefficient takes values 0.72 for conical indenters and

18 0.75 for spheres at small depths. The contact stiffness S is the measured initial slope of the unloading

19 force-displacement curve; it follows from the elastic modulus through the equation:

$$S = 2\beta \sqrt{\frac{A}{\pi}} E_r$$

1   with β a correction coefficient equal to 1 for axisymmetric indenters and E_r the "reduced" modulus

2   obtained from the indented material moduli E and ν, and the indenter tip moduli E_i and ν_i (usually

3   diamond):

$$\frac{1}{E_r} = \frac{1 - \nu^2}{E} + \frac{1 - \nu_i^2}{E_i}$$

4

5   Although sharp pyramidal indenters are widely used in this context, spherical indentation allows for

6   primarily elastic contact for shallow indents [25] and is preferred here for to perform property mapping

7   at high spatial resolution and with therefore small probed volumes. The scale dependency of the

8   spherical indentation (due to the non-self-similarity of the geometry) also allows to study the amount

9   of irreversible strain relatively to elasticity for a given loading path.

10   **b. Gaussian mixture property decomposition and issues**

11   Given the random nature of the probed areas under the indenter (heterogeneity, residual roughness)

12   the statistical indentation technique is the usual way to analyze nanoindentation data on cementitious

13   materials [15]. The technique essentially consists in fitting the mechanical properties experimental

14   statistical distribution with a weighted sum of Gaussian functions, known as a Gaussian Mixture Model

15   (GMM). This fit is a highly dimensional optimization problem (a two-component GMM in two-

16   dimensions has 7 parameters) commonly solved using the Expectancy-Maximization (EM) algorithm

17   [26].

18   One may consider a simple numerical experiment based on a simple statistical model for the

19   indentation modulus on a two-phase material. Let us consider that the effective indentation modulus

20   measured in a biphasic area is given by the Voigt (uniform strain) bound [27], to which is added some

21   error term. For a uniform Poisson's ratio, it yields the simple rule of mixtures:

22

$$E_{eff} = f E_1 + (1 - f) E_2 + e$$

1   where E_1 is the indentation modulus of phase "1", f its volume fraction in the probed volume and e a

2   measurement error. One may check that using the Reuss (uniform stress) bound does not yield

3   significantly different conclusions for the range of parameters chosen here. This random variable is

4   obtained from the random variables E_1, E_2 and e, which will assumed to follow a normal distribution

5   and f which is assumed to follow a beta distribution, with probability density:

6
$$\beta(x) = \frac{x^{a-1}(1-x)^{b-1}}{B(a,b)}$$

7   with B the beta function which is the proper normalization constant. Parameters a and b define the

8   shape of this distribution. The beta distribution allows for general modelling of a continuous random

9   variable on $[0,1]$ and is therefore well adapted to the statistical behavior of proportions. In our case,

10   we assume that indents in nearly homogenous areas are highly probable (f very likely to be close to 0

11   or 1) and therefore $a \ll 1$ and $b \ll 1$. Phase "1" is also assumed to be of higher volume fraction than

12   phase "2" (hence, f is more likely to be close to 1 than 0) and therefore $a < b$.

13   As a numerical application, we assume phases with mechanical properties similar to the two usually

14   considered types of C-S-H [28,29] and chose E_1 and E_2 to follow a Gaussian distribution with means

15   18 and 28 GPa and standard deviation 4 GPa (Figure 1). This assumption matters since we assume

16   phases have an intrinsic dispersion in mechanical properties and that the final statistical dispersion is

17   only partially due to heterogeneous probed volumes. The error e is taken from a centered Gaussian

18   distribution with standard deviation 1 GPa. Finally, coefficients for the beta distribution are taken

19   arbitrarily as $a = 0,017$ and $b = 0,035$ which results in a probability of f to be in $[0, 0.01]$ of

20   approximately 62% and 28% between $[0.99, 1]$(Figure 1). Having 10% of indents in somewhat

21   heterogeneous areas is voluntarily an extremely optimistic model that assumes that the experiment is
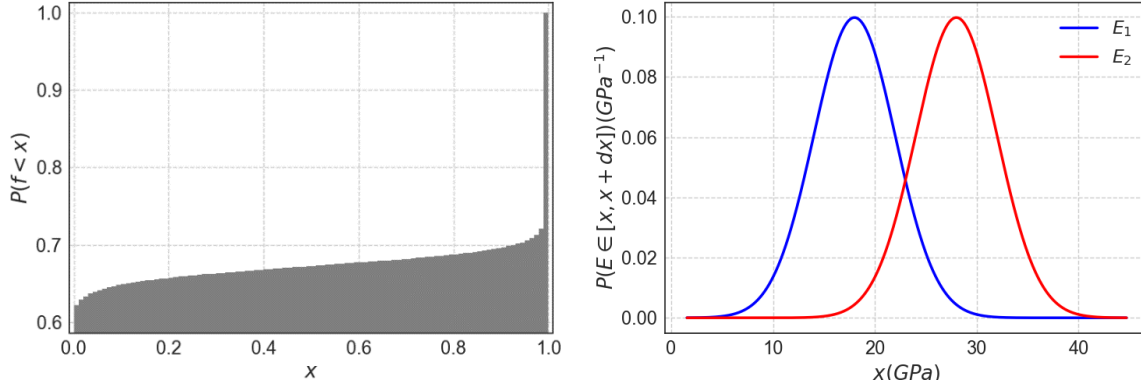
22   properly designed [22].

Figure 1: Cumulative distribution function selected for f (left), probability density functions selected for E_1 and E_2 (right).

Datasets with 1000 modulus measurements are then generated as they appear empirically to be a reasonable amount of data to differentiate phases in cementitious materials. A two-component Gaussian mixture model is then fitted to this data with the usual EM algorithm, as it can be observed for a dataset in Figure 2. One expects to recover the correct means of the E_1 and E_2 distributions as the two means of the Gaussian mixture components, at least as a limit for a large number of repeated experiments.
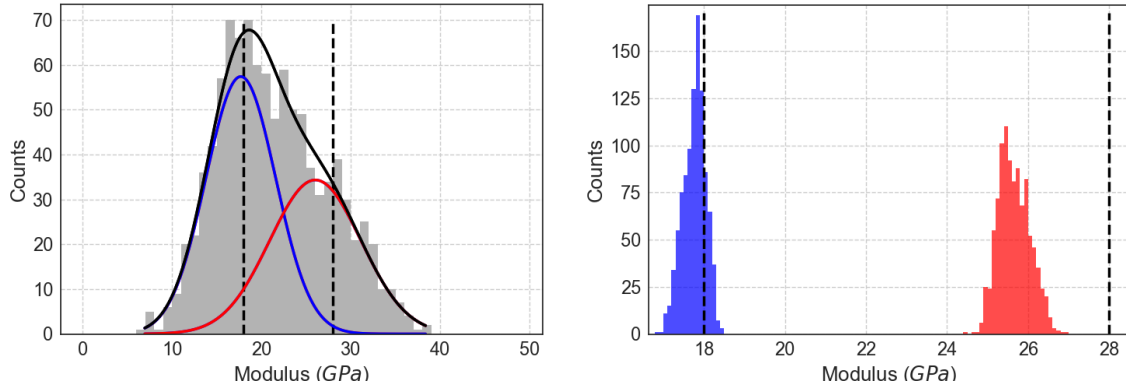

Figure 2: One realization of the E_{eff} distribution for 1000 indents and associated best Gaussian mixture fit (left), distributions of average values of the Gaussian components fitted for 1000 experiments with 1000 indents each (right).

For 1000 experiments each containing 1000 indents, the fit of a Gaussian mixture model with two components is performed. The distribution of the means of these Gaussian curves is represented in Figure 2: it can be observed in particular that these means generally underestimate the means of the original phase distributions; finding the correct average value for the stiff phase modulus has actually almost zero probability. The most likely value is around 25.4 GPa, to be compared to the expected 28 GPa; the estimated weight (volume fraction) of the soft phase is approximately 55% as compared to the expected 67% (as defined as the value of the cumulative distribution function of f at 50%). However, one may check that constraining either the weights (phase volume fractions) or means of the Gaussian components would yield correct values for the free parameters, which is characteristic of an underdetermined problem. As a conclusion, with fairly reasonable assumptions about the statistics of nanoindentation results (two phases, separated with moderate overlap, moderate heterogeneity, low experimental errors), it can be observed that results yielded by Gaussian mixture phase decomposition do not generally converge to the correct average values for the phases properties (both mechanical properties and phase fractions), even for an unrealistic large number of experiments. This type of method may converge to many local minima as shown by [22], and the model parameters at the global minimum do not generally coincide with the sample generating distribution parameters. The potential bias of the method in the case where more than two phases partially overlap (for example in cementitious matrices with portlandite CH around 40 GPa and stiffer anhydrous phases), or have non-Gaussian distributions, may be significantly high.

3. Alternative method : hierarchical clustering applied to nanoindentation

In view of the previous results, it is useful to attribute phases to each indent based on the properties of the force-displacement curves themselves instead of identifying phase probability distributions on the whole dataset. With no *a priori* knowledge about the mechanical properties of each phase, one may use unsupervised clustering algorithms, a class of algorithms aiming to regroup automatically data vectors into classes based on some similarity measure. Moreover, the usual decomposition method

7

1 makes no use of spatial correlations of the dataset that arises when the experiment is properly

2 designed (indent spacing adequately small - lower than the characteristic heterogeneity size). In

3 particular, indents in heterogeneous areas can be detected as small scale variations in measured

4 mechanical properties, and spatially close areas with similar mechanical properties are likely to be

5 from the same phase. The proposed algorithm attempts to take into account these remarks.

6 **a. Data preprocessing**

7 Each indentation force-displacement curve is summarized as a vector that describes as completely as

8 possible its properties with minimal data. To each point ("observation") from an indent is associated

9 the vector X:

10 $$X = [x, y, E, H, h_r, R]$$

11 Where x and y are the spatial coordinates of the indent, E and H the usual indentation modulus and

12 hardness, h_r the residual depth and R the ratio of the elastic strain energy to the total strain energy,

13 that is linked to the compared curvatures of the loading and unloading curves. R is calculated as the

14 ratio of the integrals of the force-displacement unloading branch and the loading branch. Although

15 large (non-linear) correlations exist between these quantities, they are not entirely redundant: no data

16 reduction procedure (such as Principal Component Analysis, for example) is attempted. Data remains

17 of reasonable dimensionality, unlike datasets with many descriptors given for example by Acoustic

18 Emission signals [30]. Moreover, using an enriched dataset relatively to the usual $[E, H]$ is expected to

19 provide additional robustness into the method when dealing with noisy or imperfectly corrected data:

20 R is notably invariant through a shift in displacement and insensitive to small errors in zero-point

21 correction.

22 The local relative error of the indentation hardness is computed as the ratio of the standard deviation

23 S to the mean μ of hardness values in a neighborhood (called H^x):

$$1 \qquad\qquad s(H,x) = \frac{S(H^x)}{\mu(H^x)}$$

2   Where the neighborhood is chosen here as the indent itself and its four nearest neighbors. This

3   parameter characterizes the local variability in mechanical properties. The physical size of the

4   neighborhood should be smaller than the characteristic heterogeneity length scale. In order to

5   eliminate probably heterogeneous regions, indents are eliminated from the analysis if $s(H)$ is higher

6   than some arbitrarily defined value; in the present work, indents must verify $s(H,x) < 25\%$.

7   Finally, since X components are of different magnitudes and are to be compared, each measured

8   quantity is normalized such that the whole dataset is of mean 0 and variance 1 for each component.

9   **b. Clustering algorithm**

10   The selected clustering algorithm is of agglomerative hierarchical type [31]: with initially each

11   observation belonging to its own cluster ("singlet"), clusters are successively merged until the final

12   number of required clusters is reached. At each step, merging is performed according to some criterion

13   which aims at globally achieving maximal similarity of elements inside each cluster and maximal

14   dissimilarity between clusters (or, geometrically, maximal intra-cluster compacity and inter-cluster

15   separation). We use the weighted Euclidean distance as a similarity measure in the 6D space of data

16   vectors:

$$17 \qquad\qquad d(X^a, X^b) = \sqrt{\sum_{i=1}^{6} w_i^2 (X_i^a - X_i^b)^2}$$

18   The weights w_i are introduced in order to adjust the influence the different measured quantities on

19   the similarity measure. All mechanical parameters are treated equally but spatial coordinates are

20   chosen to have a reduced influence when selecting the clusters to merge. Therefore we choose in the

21   present case $w_1^2 = w_2^2 < 1$, all other weights being kept to 1.

1   The selected algorithm is Ward's method [32]; at each merging step, one selects the couple of clusters

2   to merge such that the increase in intra-cluster "inertia" is minimal, defined as:

3

$$I_{intra} = \frac{1}{N} \sum_{i=1}^{k} \sum_{j=1}^{N_i} d(X^j - \chi^i)^2$$

4   where we have at the current step N observations in k clusters with each N_i elements, and center of

5   gravity χ^i (such as defined with the aforementioned distance). For a given dataset and distance, the

6   final cluster hierarchy is unique: it does not depend on any initialization of the algorithm or on the

7   number of clusters to be found. The final number of clusters k (where to "stop" the merging process)

8   in the dataset must however be selected or deduced from some clustering quality evaluation

9   parameter (such as [33]). The interest of the method is that one takes into account the fact that indents

10   in the same phases should be similar in mechanical properties but also spatially close; using different

11   wording, two distant points, to be affected to the same cluster, have to exhibit very similar mechanical

12   properties.

13   **4. Application**

14   **a. Materials and methods**

15   Two different materials are tested: firstly a CEM I cement paste with water-to-cement ratio of 0.52

16   (see, for example, [34]) (Figure 3); secondly a hydrated C3S (alite) paste with identical water-to-cement

17   ratio (Figure 4). In both cases a small sample was extracted from a large mature sample and was

18   mounted in epoxy resin, grinded and polished with a final step during one hour in an alcohol based

19   diamond suspension with average grain size 0.25 μm, in order to reach adequate surface quality.
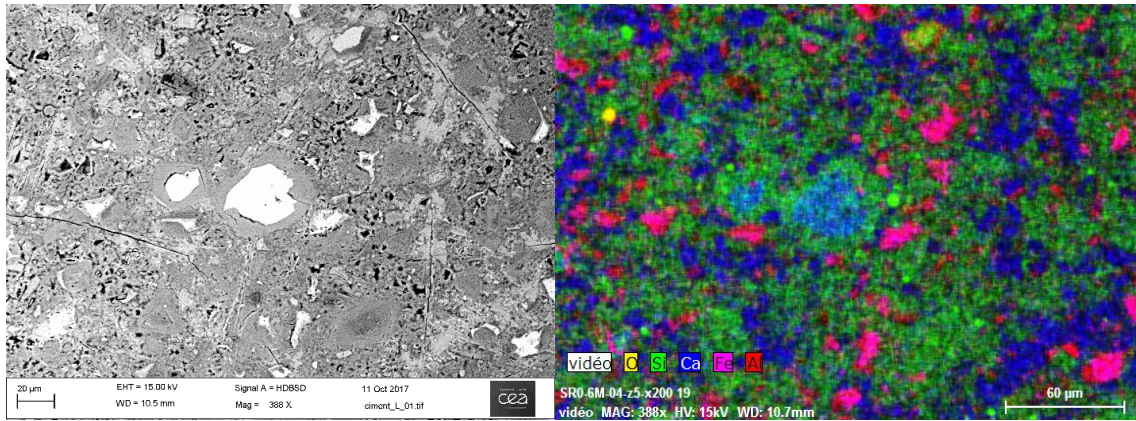
20

Figure 3: Backscattered electron microscope image at 388x of a freeze-dried similar sample of cement paste and composite Si+Ca+Fe+Al (+O) Energy Dispersive X-ray Spectroscopy elemental map of the area. Usual phases are observed in SEM-EDS maps: C-S-H, (green), portlandite (CH, blue), anhydrous residual cement grains (cyan), and other minor hydration products (red and pink).
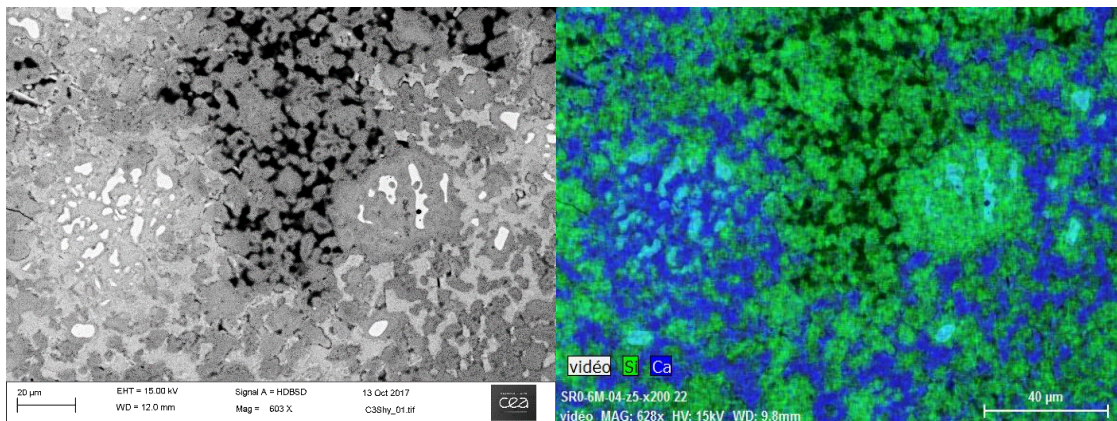

Figure 4: Backscattered electron microscope image at 603x of a freeze-dried similar sample of hydrated C3S and composite Si+Ca Energy Dispersive X-ray Spectroscopy elemental map of the area. Observed phases are C-S-H (green), portlandite (CH, blue), anhydrous C3S (cyan), and mesoporosity (black).

The microstructures are observed to be quite different: the mesoporosity in hydrated alite is coarser and clustered in very porous regions of some 100 µm in size (Figure 4). However, the properties of the

1   two C-S-H types have been shown not to depend on the material composition; only the volume

2   fractions are expected to vary [3] which is the basis for comparing both materials' phases properties.

3   The datasets on cement paste and hydrated alite were obtained from respectively 32×32 and 32×38

4   indentation grids of spacing 2 μm acquired with a 10 μm radius spherical diamond indenter and a

5   Zwick-Roell ZHN/SEM® (Ulm, Germany) nanoindenter in the laboratory conditions, with maximum

6   force 2 mN.

7   **b. Results on cement paste**

8   The resulting maps of the indentation modulus, hardness, residual depth and elastic-to-total strain

9   energy ratio are presented in Figure 5. The resulting mapping of a 64 μm × 64 μm area shows relatively

10   homogeneous subdomains of approximately 10-20 μm that can visually be attributed to 4 different

11   phases of distinct mechanical properties. The probed area may be too small to constitute a

12   representative sample of the cement paste mechanical properties, especially in terms of phase volume

13   fractions, although microstructure data yields comparable orders of magnitude [35,36]. The elastic-

14   to-total strain energy ratio (R) map allows to distinguish phases with properties around the values 0.3,

15   0.5, 0.65 and 0.8. The standard analysis of statistical nanoindentation has been applied to this 1024

16   point dataset and a Gaussian mixture model with three components fitted (with full covariance matrix)

17   to the (E, H) results using the implementation of Python module scikit-learn [37]. The distribution

18   components and (E, H) data are presented in Figure 6 and numerical parameters in Table 1.

19   It can be observed for this sample that phases are not clearly separated in the data histograms and

20   that issues of the type presented in 2.b may be expected, as a large number of models may yield fits

21   as adequate as the global optimum presented here. In particular, one may check that using a four

22   component Gaussian mixture yields optima with components of comparable weights and largely

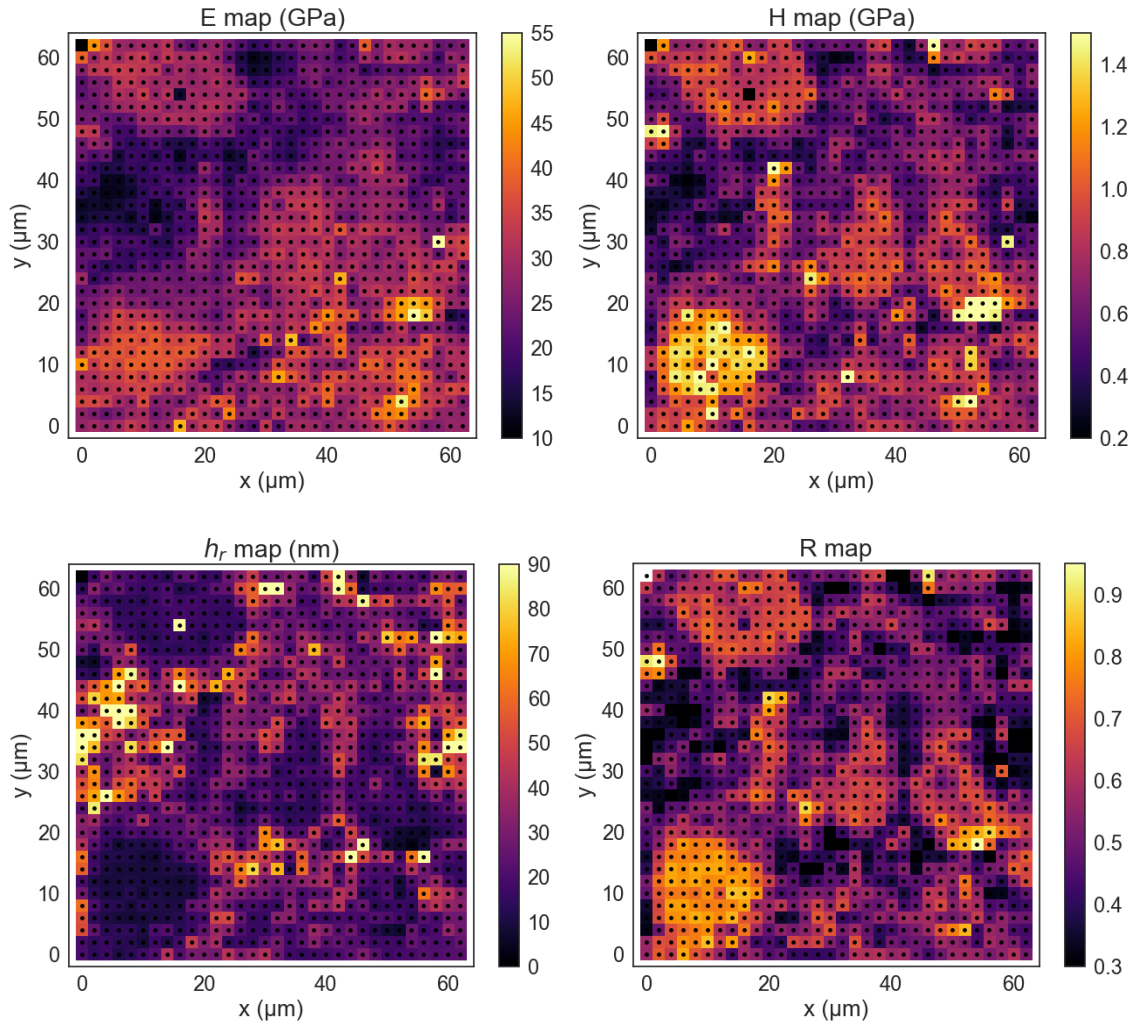23   overlapping, which constitutes an even worse decomposition of the material phase's properties.

24

Figure 5: Maps of the indentation modulus, indentation hardness, residual depth and elastic-to-total

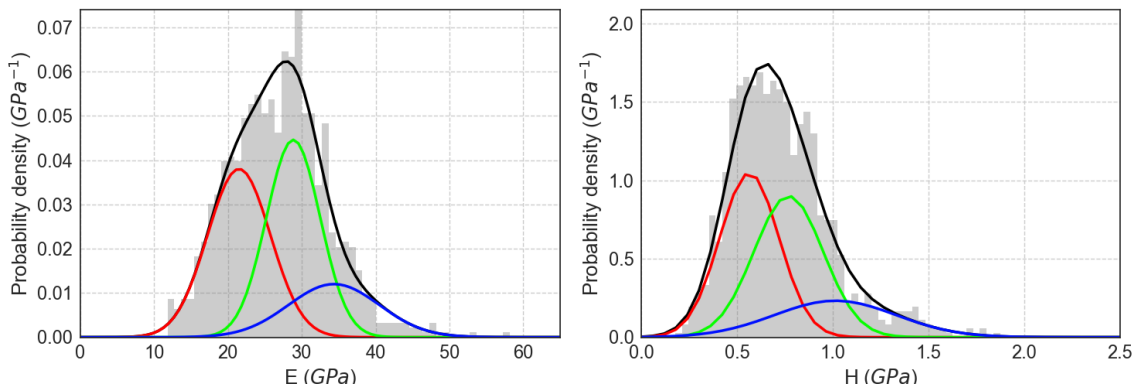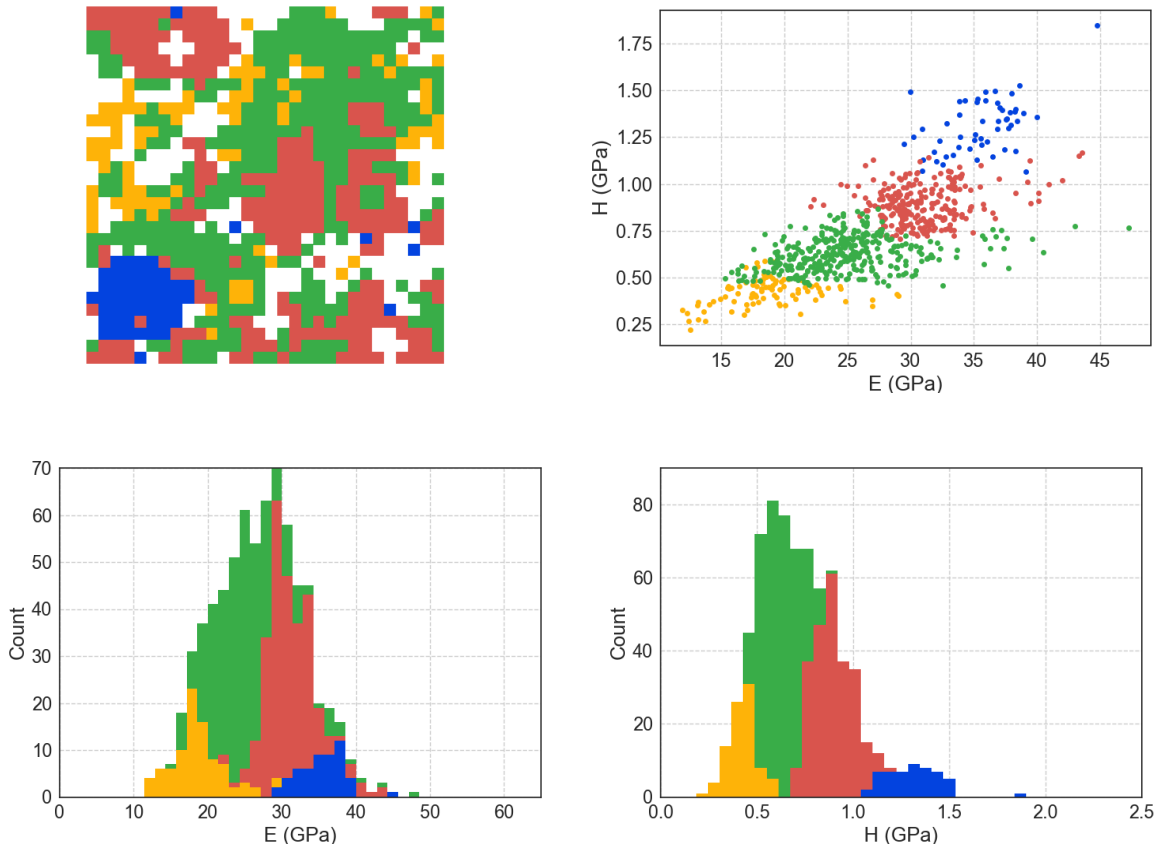strain energy ratio (R) on a cement paste sample using spherical nanoindentation.

Figure 6: Obtained 2D Gaussian mixture using the standard method, fit projected onto the E and H

axes.

	Weight	E (GPa)	H (GPa)
Component 1	41%	21 ± 4.3	0.56 ± 0.15
Component 2	41%	29 ± 3.6	0.77 ± 0.18
Component 3	19%	34 ± 6.2	1.01 ± 0.32

1 *Table 1 : Properties of the three component optimal Gaussian mixture model fitted to the data, with*

2 *standard deviations given as errors.*

3 The proposed method is then applied to the analysis of this dataset using empirically defined weights

4 $w_1{}^2 = w_2{}^2 = 0.2$ also implemented from the Python module scikit-learn [37]. In order to calculate in

5 each point the local variability criterion, the outer indents are excluded from the analysis and therefore

6 the studied dataset makes use of 900 indents; moreover the criterion excludes 181 points from the

7 subsequent steps (21% of the dataset). The 719 remaining indents are classified using the hierarchical

8 algorithm described above and results for the $k = 4$ cluster number are represented in Figure 7.

9

10

11

12

13

14

Figure 7: Obtained clustering in physical space (map), in the (E, H) plane, and E and H distributions per phase as stacked histograms for cement paste.

The obtained per phase property distributions are "irregular" and unsymmetrical and cannot be accurately fitted with Gaussian distributions. The clustering results for $k = 4$ shows that areas excluded from the analysis are mostly of "weaker" mechanical properties that may correspond to roughness due to local porosity and/or damage, and their sizes are consistent with the porosity sizes observed in the electron microscopy images (few micrometers, Figure 3) and also to isolated indents with high mechanical properties, that may be attributed to minor hydration products or anhydrous phases. The procedure yields necessarily well separated clusters that optimize the prescribed criterion of separation in the space of mechanical properties mixed with some preference for local space compacity. The properties of the four phases are given in Table 2.

	Weight	E (GPa)	H (GPa)	Attribution
Cluster 0 (yellow)	12%	19 ± 3.5	0.42 ± 0.07	High porosity area
Cluster 1 (green)	46%	25 ± 4.6	0.63 ± 0.09	OP C-S-H
Cluster 2 (red)	34%	31 ± 3.2	0.89 ± 0.10	IP C-S-H
Cluster 3 (blue)	7%	35 ± 2.9	1.31 ± 0.14	CH

1 *Table 2 : Properties of the four clusters found using the proposed algorithm, with standard deviations*

2 *given as errors.*

3 The size of the studied example area being relatively small, the representativity of the sample may be

4 too weak for definitive results, especially regarding the volume fractions. At the studied high water-

5 to-cement ratio, the need to separate very high porosity areas from the commonly defined "outer

6 product (OP)" and "inner product (IP)" C-S-H is confirmed [28] although most of it is already eliminated

7 when considering our criterion of local homogeneity. These very high porosity areas are clustered in

8 Cluster 0. Cluster 1, 2 and 3 may therefore be classically attributed to respectively OP C-S-H, IP C-S-H

9 and portlandite (CH), with consistent mechanical properties with those reported in the literature

10 [28,29].

11 **c. Application to hydrated C3S**

12 The phases are less clearly separated in this example (Figure 8) and the selected area does not contain

13 a highly mesoporous zone. The distribution of indentation properties can also be seen to be almost

14 unimodal and can be shown to be accurately fitted with a single Gaussian component, hence negating

15 the capabilities of the standard statistical indentation technique. For a selected ponderation

16 parameter $w_i{}^2$ the proposed method yields a unique classification for a given number of clusters.

17 Excluding the edges and the indents violating the local homogeneity criterion, 1035 points are
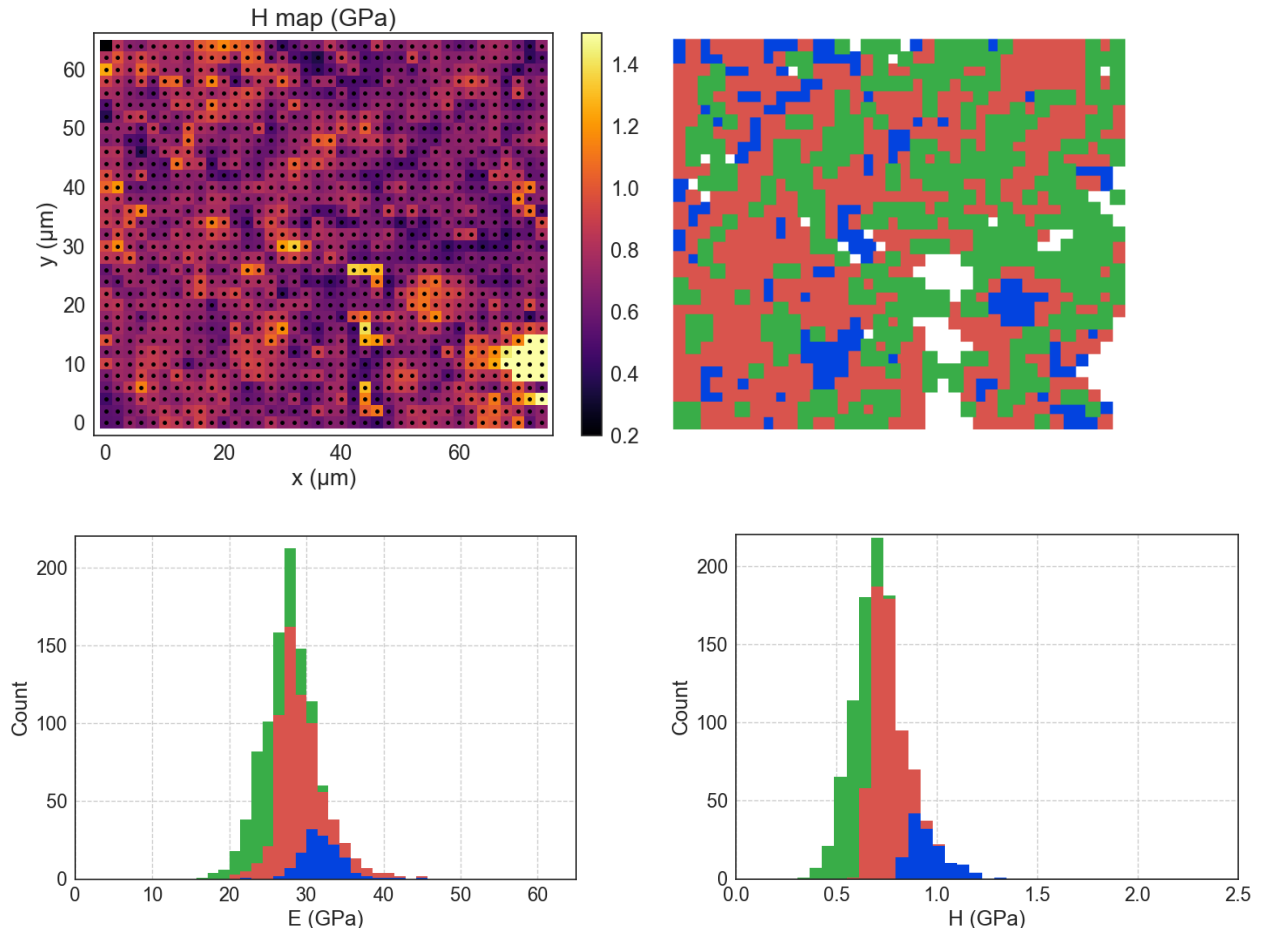
18 classified.

16

Figure 8: Map of the indentation hardness, obtained clustering in physical space, and E and H distributions per phase as stacked histograms for hydrated C3S.

	Weight	E (GPa)	H (GPa)	Attribution
Cluster 1 (green)	35%	25 ± 2.8	0.59 ± 0.07	OP C-S-H
Cluster 2 (red)	52%	29 ± 3.0	0.65 ± 0.09	IP C-S-H
Cluster 3 (blue)	13%	32 ± 3.0	0.96 ± 0.10	CH

Table 3 : Properties of the four clusters found using the proposed algorithm, with standard deviations given as errors.

The result for $k = 3$ is reported in Table 3. The determined clusters possess mechanical properties consistent with those numbered 1 to 3 in cement paste (Table 2) that were attributed respectively to

OP C-S-H, IP C-S-H and CH (portlandite), without the need to separate in the analysis very porous areas, consistenty with the observations of [3]. This application confirms the main interest of the method : phases are unambiguously classified when no obvious separation in the (E, H) histograms exist.

5. Conclusions

A classification method based on a classical hierarchical clustering algorithm has been applied to nanoindentation results, using enriched information: to the usual indentation hardness and modulus is added additional mechanical parameters and spatial position of the indent. This method has been shown to:

1. Allow an identification of phases on nanoindentation results that is model independent (no need for Gaussian properties distribution or widely separated phases), and identify each point unambiguously (instead of deriving a probability distribution for each phase),

2. Allow eliminating points in areas that may be largely porous or heterogeneous.

As a perspective, this method can be extended in a straightforward manner to "multichannel" maps obtained using other experimental techniques. It will require the definition of suitable components to the data vector and an updated distance function. It may include compositional information such as elemental ratios (SEM-EDS), density/average atomic number (SEM-backscattered imaging gray level) or molecular composition and structure (Raman microspectroscopy) that would allow an increased reliability of the phase separation as well as establishing correlations between the local measured quantities. If the properties of Gaussian Mixture Models are desirable (smooth distributions of properties) the hierarchical clustering method presented here may also be used to initialize or constrain fit parameters (such as the means) when many local minima are expected.

6. Acknowledgements

7. References

[1] P. Mondal, S.P. Shah, L.D. Marks, Nanomechanical Properties of Interfacial Transition Zone in Concrete, in: Nanotechnol. Constr. 3, Springer, Berlin, Heidelberg, 2009: pp. 315–320. doi:10.1007/978-3-642-00980-8_42.

[2] W. Zhu, P.J.M. Bartos, Application of depth-sensing microindentation testing to study of interfacial transition zone in reinforced concrete, Cem. Concr. Res. 30 (2000) 1299–1304. doi:10.1016/S0008-8846(00)00322-7.

[3] G. Constantinides, F.-J. Ulm, The effect of two types of C-S-H on the elasticity of cement-based materials: Results from nanoindentation and micromechanical modeling, Cem. Concr. Res. 34 (2004) 67–80. doi:10.1016/S0008-8846(03)00230-8.

[4] J. Han, G. Pan, W. Sun, C. Wang, D. Cui, Application of nanoindentation to investigate chemomechanical properties change of cement paste in the carbonation reaction, Sci. China Technol. Sci. 55 (2012) 616–622. doi:10.1007/s11431-011-4571-1.

[5] J. Frech-Baronet, L. Sorelli, J.-P. Charron, New evidences on the effect of the internal relative humidity on the creep and relaxation behaviour of a cement paste by micro-indentation techniques, Cem. Concr. Res. 91 (2017) 39–51. doi:10.1016/j.cemconres.2016.10.005.

[6] C. Pichler, R. Lackner, Identification of Logarithmic-Type Creep of Calcium-Silicate-Hydrates by Means of Nanoindentation, Strain. 45 (2009) 17–25. doi:10.1111/j.1475-1305.2008.00429.x.

[7] M. Vandamme, F.-J. Ulm, Nanoindentation investigation of creep properties of calcium silicate hydrates, Cem. Concr. Res. 52 (2013) 38–52. doi:10.1016/j.cemconres.2013.05.006.

[8] Q. Zhang, R. Le Roy, M. Vandamme, B. Zuber, Long-term creep properties of cementitious materials: Comparing microindentation testing with macroscopic uniaxial compressive testing, Cem. Concr. Res. 58 (2014) 89–98. doi:10.1016/j.cemconres.2014.01.004.

[9] G. Constantinides, F.-J. Ulm, K.V. Vliet, On the use of nanoindentation for cementitious materials, Mater. Struct. 36 (2003) 191–196. doi:10.1007/BF02479557.

[10] J.J. Hughes, P. Trtik, Micro-mechanical properties of cement paste measured by depth-sensing nanoindentation: a preliminary correlation of physical properties with phase type, Mater. Charact. 53 (2004) 223–231. doi:10.1016/j.matchar.2004.08.014.

[11] P. Mondal, S.P. Shah, L. Marks, A reliable technique to determine the local mechanical properties at the nanoscale for cementitious materials, Cem. Concr. Res. 37 (2007) 1440–1444. doi:10.1016/j.cemconres.2007.07.001.

[12] K. Velez, S. Maximilien, D. Damidot, G. Fantozzi, F. Sorrentino, Determination by nanoindentation of elastic modulus and hardness of pure constituents of Portland cement clinker, Cem. Concr. Res. 31 (2001) 555–561. doi:10.1016/S0008-8846(00)00505-6.

[13] Y. Wei, S. Liang, X. Gao, Phase quantification in cementitious materials by dynamic modulus mapping, Mater. Charact. 127 (2017) 348–356. doi:10.1016/j.matchar.2017.02.029.

[14] O. Bernard, F.-J. Ulm, E. Lemarchand, A multiscale micromechanics-hydration model for the early-age elastic properties of cement-based materials, Cem. Concr. Res. 33 (2003) 1293–1309. doi:10.1016/S0008-8846(03)00039-5.

[15] G. Constantinides, K.S. Ravi Chandran, F.-J. Ulm, K.J. Van Vliet, Grid indentation analysis of composite microstructure and mechanics: Principles and validation, Mater. Sci. Eng. A. 430 (2006) 189–202. doi:10.1016/j.msea.2006.05.125.

[16] F.-J. Ulm, M. Vandamme, C. Bobko, J. Alberto Ortega, K. Tai, C. Ortiz, Statistical Indentation Techniques for Hydrated Nanocomposites: Concrete, Bone, and Shale, J. Am. Ceram. Soc. 90 (2007) 2677–2692. doi:10.1111/j.1551-2916.2007.02012.x.

[17] J.J. Chen, L. Sorelli, M. Vandamme, F.-J. Ulm, G. Chanvillard, A Coupled Nanoindentation/SEM-EDS Study on Low Water/Cement Ratio Portland Cement Paste: Evidence for C–S–H/Ca(OH)2 Nanocomposites, J. Am. Ceram. Soc. 93 (2010) 1484–1493. doi:10.1111/j.1551-2916.2009.03599.x.

[18] K. J. Krakowiak, W. Wilson, S. James, S. Musso, F.-J. Ulm, Inference of the phase-to-mechanical property link via coupled X-ray spectrometry and indentation analysis: Application to cement-based materials, Cem. Concr. Res. 67 (2015) 271–285. doi:10.1016/j.cemconres.2014.09.001.

[19] W. Wilson, L. Sorelli, A. Tagnit-Hamou, Automated coupling of NanoIndentation and Quantitative Energy-Dispersive Spectroscopy (NI-QEDS): A comprehensive method to disclose the micro-chemo-mechanical properties of cement pastes, Cem. Concr. Res. 103 (2018) 49–65. doi:10.1016/j.cemconres.2017.08.016.

[20] P. Trtik, B. Münch, P. Lura, A critical examination of statistical nanoindentation on model materials and hardened cement pastes based on virtual experiments, Cem. Concr. Compos. 31 (2009) 705–714. doi:10.1016/j.cemconcomp.2009.07.001.

[21] F.-J. Ulm, M. Vandamme, H.M. Jennings, J. Vanzo, M. Bentivegna, K.J. Krakowiak, G. Constantinides, C.P. Bobko, K.J. Van Vliet, Does microstructure matter for statistical nanoindentation techniques?, Cem. Concr. Compos. 32 (2010) 92–99. doi:10.1016/j.cemconcomp.2009.08.007.

[22] P. Lura, P. Trtik, B. Münch, Validity of recent approaches for statistical nanoindentation of cement pastes, Cem. Concr. Compos. 33 (2011) 457–465. doi:10.1016/j.cemconcomp.2011.01.006.

[23] W.C. Oliver, G.M. Pharr, An improved technique for determining hardness and elastic modulus using load and displacement sensing indentation experiments, J. Mater. Res. 7 (1992) 1564–1583. doi:10.1557/JMR.1992.1564.

[24] I.N. Sneddon, The relation between load and penetration in the axisymmetric boussinesq problem for a punch of arbitrary profile, Int. J. Eng. Sci. 3 (1965) 47–57. doi:10.1016/0020-7225(65)90019-4.

[25] A.J. Bushby, Nano-Indentation Using Spherical Indenters, Nondestruct. Test. Eval. 17 (2001) 213–234. doi:10.1080/10589750108953112.

[26] A.P. Dempster, N.M. Laird, D.B. Rubin, Maximum Likelihood from Incomplete Data via the EM Algorithm, (1976). https://dash.harvard.edu/handle/1/3426318 (accessed February 1, 2018).

[27] N.X. Randall, M. Vandamme, F.-J. Ulm, Nanoindentation analysis as a two-dimensional tool for mapping the mechanical properties of complex surfaces, J. Mater. Res. 24 (2009) 679–690. doi:10.1557/jmr.2009.0149.

[28] C. Hu, Y. Han, Y. Gao, Y. Zhang, Z. Li, Property investigation of calcium–silicate–hydrate (C–S–H) gel in cementitious composites, Mater. Charact. 95 (2014) 129–139. doi:10.1016/j.matchar.2014.06.012.

[29] C. Hu, Z. Li, A review on the mechanical properties of cement-based materials measured by nanoindentation, Constr. Build. Mater. 90 (2015) 80–90. doi:10.1016/j.conbuildmat.2015.05.008.

[30] M. Moevus, N. Godin, M. R'Mili, D. Rouby, P. Reynaud, G. Fantozzi, G. Farizy, Analysis of damage mechanisms and associated acoustic emission in two SiC$_f/$[Si-B-C] composites exhibiting different tensile behaviours. Part II: Unsupervised acoustic emission data clustering, Compos. Sci. Technol. 68 (2008) 1258–1265.

[31] A.K. Jain, M.N. Murty, P.J. Flynn, Data Clustering: A Review, ACM Comput Surv. 31 (1999) 264–323. doi:10.1145/331499.331504.

[32] J. Ward Jr., Hierarchical grouping to optimize an objective function, J. Am. Stat. Assoc. 58 (1963) 236–244.

[33] D.L. Davies, D.W. Bouldin, A Cluster Separation Measure, IEEE Trans. Pattern Anal. Mach. Intell. PAMI-1 (1979) 224–227. doi:10.1109/TPAMI.1979.4766909.

[34] A. Aili, Shrinkage and creep of cement-based materials under multiaxial load : poromechanical modeling for application in nuclear industry, PhD Thesis, Université Paris-Est, 2017. https://pastel.archives-ouvertes.fr/tel-01682129/document (accessed February 13, 2018).

[35] N. Ukrainczyk, E.A.B. Koenders, K. van Breugel, Representative Volumes for Numerical Modeling of Mass Transport in Hydrating Cement Paste, in: Multi-Scale Model. Charact. Infrastruct. Mater., Springer, Dordrecht, 2013: pp. 173–184. doi:10.1007/978-94-007-6878-9_13.

1   [36] M.H.N. Yio, H.S. Wong, N.R. Buenfeld, Representative elementary volume (REV) of cementitious
2   materials from three-dimensional pore structure analysis, Cem. Concr. Res. 102 (2017) 187–202.
3   doi:10.1016/j.cemconres.2017.09.012.
4   [37] F. Pedregosa, G. Varoquaux, A. Gramfort, V. Michel, B. Thirion, O. Grisel, M. Blondel, P.
5   Prettenhofer, R. Weiss, V. Dubourg, J. Vanderplas, A. Passos, D. Cournapeau, M. Brucher, M.
6   Perrot, É. Duchesnay, Scikit-learn: Machine Learning in Python, J. Mach. Learn. Res. 12 (2011)
7   2825–2830.
8